Creep and aging of hard-sphere glasses under constant stress

P. Ballesta[1,2,*] and G. Petekidis[2,3]

[1]*Faculdade de Engenharia da Universidade do Porto - CEFT - Dep. Engenharia Química, Rua Dr. Roberto Frias, 4200-465 Porto, Portugal*

[2]*IESL-FORTH, PO Box 1527, Heraklion 71110, Crete, Greece*

[3]*Department of Materials Science & Technology, University of Crete, Greece*

(Received 29 June 2015; revised manuscript received 16 February 2016; published 25 April 2016)

We investigate the aging behavior of glassy suspensions of nearly hard-sphere colloids submitted to a constant shear stress. For low stresses, below the yield stress, the system is subject to creep motion. As the sample ages, the shear rate exhibits a power-law decrease with time with exponents that depend on the sample age. We use a combination of rheological experiments with time-resolved photon correlation spectroscopy to investigate the time evolution of the sample dynamics under shear on various time and length scales. Long-time light-scattering experiments reveal the occurrence of microscopic rearrangement events that are linked with the macroscopic strain deformation of the sample. Dynamic time sweep experiments indicate that while the internal microscopic dynamics slow down continuously with waiting time, the storage and loss moduli are almost constant after a fast, weak decrease, resembling the behavior of quenched systems with partially frozen-in stresses.

DOI: 10.1103/PhysRevE.93.042613

I. INTRODUCTION

In arrested states the relaxation time diverges and no long-range rearrangements take place during the experimental timescale. Such arrested (or nonergodic) states can be reached either due to a change in inherent system parameters such as volume fraction or cross-linking or of external conditions such as shear or temperature (or pressure for molecular fluids) [1]. Colloidal suspensions exhibit, in general, two arrested states: For hard-sphere or repulsive interactions, the relaxation time related with out-of-cage motion (termed α relaxation) diverges when the volume fraction, ϕ, approaches a glass transition volume fraction, ϕ_g [2,3], due to an entropic hindrance (or caging) exerted to a particle by its neighbors. For attractive colloids, the divergence takes place at a critical attraction strength [4,5], beyond which gel states are formed due to the formation of an interconnected network of bonded particles.

The time evolution and aging of such arrested phases (glasses and gels) is one of the main ongoing subjects in soft-matter science [3,6–8]. Aging of colloidal suspensions, glasses, or gels is often studied using light-scattering techniques, where taking advantage of large ensemble averaging the internal dynamics can be followed at rest [3,9–12], after [13–15] or during shear [16], and by rheological studies where the mechanical properties can be monitored as a function of waiting time [8,17,18].

With regard to their mechanical response, colloidal suspensions above ϕ_g or for attractions higher than the critical gel transition exhibit a liquid to solid transition acquiring a yield stress [19–21], σ_y, at least for timescales shorter than the experimental one. Therefore, for stresses below σ_y the system exhibits a solid-like response, which ideally would enforce a zero shear rate condition, when a certain strain (or deformation) is reached. However, in reality glassy colloidal systems do show a slow creeping motion when subjected to stresses below the yield stress as pointed out experimentally [1,19,20,22–27] and theoretically for thermal [25,28,29] and athermal [30] systems. Such prolonged creeping motion has been observed in glassy states of soft core-shell particles [31,32] as well as interpenetrating multiarm star polymers [33]; in the latter a very slow creep flow under low shear stress does eventually lead to an almost constant strain plateau, an effect that has been attributed to an interplay between aging and shear. The slow creep motion at stresses below the yield stress may therefore be related to local stress-induced internal rearrangements at single particle microscopic or larger mesoscopic scales [34–36], although unambiguous experimental findings are lacking. Such complex spatiotemporal response has also been suggested within viscoplastic models of yield stress fluids, where local plastic events accompanied by nonlocal stress relaxation are responsible for the creation of localized and intermittent flow [21,37]. Furthermore, although the increase of the slowest relaxation time in colloidal glasses observed by dynamic light scattering [9,10,12] would be expected to have a signature in the measured rheology, the frequency regime where linear viscoelastic measurements are mainly performed, around the plateau modulus is not significantly affected [17]. This explains why existing studies with nearly hard-sphere or short-range repulsive particles have not shown significant thixotropy [20,38,39].

In this paper we investigate aging effects on the linear and nonlinear rheology of a model system of nearly hard spheres over a period of many days. We show that time dependence is present in the linear viscoelastic moduli, albeit small compared to more common thixotropic systems with strong interparticle interactions such as colloidal gels or other soft pastes with strong attractive or repulsive interparticle interactions [40]. Measurements under constant stress, below the yield stress, reveal a prolonged creep motion (i.e., flow with progressively decreasing shear rate) as detected in various hard and soft particle glasses [7,20,25], leading after long time (and multiple strain units) to an almost ideal strain plateau. The underlying mechanism of such delayed "ideal" solid response is examined through light-scattering time-resolved photon correlation spectroscopy, stress reversal, and parallel superposition linear rheometry in order to discern the role of aging and shear-induced jamming.

*ballesta@fe.up.pt

II. EXPERIMENTAL

A. Samples

We use suspensions of polymethylmethacrylate (PMMA) colloids [41], of radius $R = 138$ nm and polydispersity $p \sim 15\%$, and of radius $R = 300$ nm and polydispersity $p \sim 12\%$, stabilized with poly-12-hydroxystearic acid, suspended in octadecene, a high boiling point (315°C) solvent, to eliminate evaporation. The higher refractive index mismatch between octadecene and PMMA ($\Delta n = 0.045$) compared to previous experiments in *cis*-decalin ($\Delta n = 0.001$) induces a weak Van der Waals attractions estimated [42,43] for two particles of radius $R = 138$ nm, separated by twice the size of the steric stabilization layer (≈ 20 nm) of $U_{VdW} = -0.09\ k_BT$. Since this attraction is far from both the repulsive-to-attractive glass transition and the reentrant liquid transitions [5] we will neglect it in the following. The high polydispersity of particles prevents crystallization and the volume fractions ϕ measured (0.6 to 0.65) are estimated by assuming a volume fraction at random close packing $\phi_{\rm rcp} = 0.67$ (± 0.005) according to previous studies [20,39].

B. Rheometry

Rheological experiments were conducted with an Anton Paar MCR-501 stress-controlled rheometer using two different geometries that gave the same results: a metallic cone-plate (10 mm radius, 2° angle) and glass plate-plate (20 mm) geometry, both thermostated by a Peltier element. Due to the high boiling point of octadecene, no solvent trap was needed to prevent evaporation. However, we found out that octadecene tends to spread on the Peltier metal bottom plate, leading to an increase of the measured viscosity and elastic moduli with time. Such delayed wetting was prevented by spreading a drop of octadecene on the bottom plate prior to sample loading, while it was completely absent in the glass plates. Under these conditions no change in the sample was observed for at least two days and up to a week.

Upon sample loading as well as before each rheological test, the sample is rejuvenated by applying a shear rate of $10\ s^{-1}$ for 600 s and then allowing it to relax for $t_w = 300$ s or 10^4 free Brownian times, $t_B = R^2/D_0 = 0.0275$ s; this leads to a reproducible well-defined state. The age of the sample t_w is fixed at zero at the end of the preshear. It should be noted that some residual stresses are expected to remain in HD glasses after shear-rate switch off (setting rate to zero) [44]. However, if stress is set to zero the system may relax by a partial strain recovery [20,45]. We measure the flow curve (stress σ versus shear rate $\dot\gamma$) from high to low shear rates. Then, we perform a dynamic frequency sweep to determine the frequency-dependent storage, G', and loss, G'', moduli in the linear regime. From the flow curve we extract the yield stress of the glassy suspension, σ_y, by fitting the experimental curve by a Herschel-Bulkley expression, $\sigma = \sigma_y[1 + (\dot\gamma\tau)^n]$. We then apply a constant stress and measure the evolution of the effective viscosity $\eta(t) = \sigma/\dot\gamma(t)$ and strain $\gamma(t)$ with time. The flow curves measured for all samples presented below are shown in Figs. 1(a) and 1(b). Note that no shear thickening was detected for all shear rates measured except for the more concentrated glass sample with the larger particles ($\phi = 0.64$ and $R = 300$ nm) and for shear rates $7\ s^{-1}$ or higher.

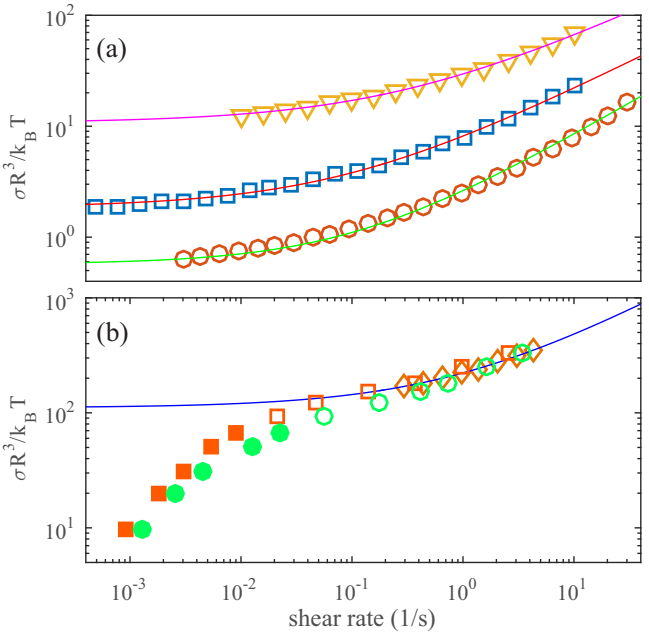

FIG. 1. (a) Flow curves of the colloidal suspensions of radius $R = 138$ nm at $\phi = 0.6$ (circles), $\phi = 0.62$ (squares), and $\phi = 0.65$, $R = 138$ nm (triangles). The continuous lines are the best fit by an Herschel-Bulkley fluid. (b) Flow curves of the colloidal suspensions of radius $R = 300$ nm and $\phi = 0.64$, at constant applied shear rate (diamonds) and extracted from the data presented in Fig. 2 for the young (circles) and aged (squares) samples 100 s after the beginning of the measurements; the full symbols are taken out of equilibrium, and the continuous line corresponds to the Herschel-Bulkley fit of the flow curve measured at constant shear-rates (continuous line).

Values of n vary in the range 0.47 for the more concentrated suspensions to 0.59 for the less concentrated ones and do not exhibit a notable dependence on the age of the sample. However, n is measured in a range of high shear rates where the sample is already sheared enough to be rejuvenated and therefore any effect of aging is either eliminated (sample rejuvenated) or is simply too small. Moreover, n depends on the sample concentration contrary to what was found in previous numerical studies [46,47], though it can be due to the limited range of shear rate studied in our experiments. Note also that some discrepancies between the absolute stress values of the flow curves of the two systems are due to different polydispersities (hence different values of the random close packing) and the standard error in the volume fraction due to preparation of different batches.

C. Light scattering

Dynamic light-scattering measurements were performed simultaneously with the long time step stress experiments. These measurements were conducted with turbid samples in the transmission geometry, with a laser light (He-Ne, $\lambda = 633$ nm) illuminating the sample through the glass parallel plate geometry (with gap of 0.2 mm) at a distance of 1.2 mm from the center of the geometry, far enough from both the center and the edge to neglect finite-size effect and edges effect. We monitor the fluctuations of the multiply scattered

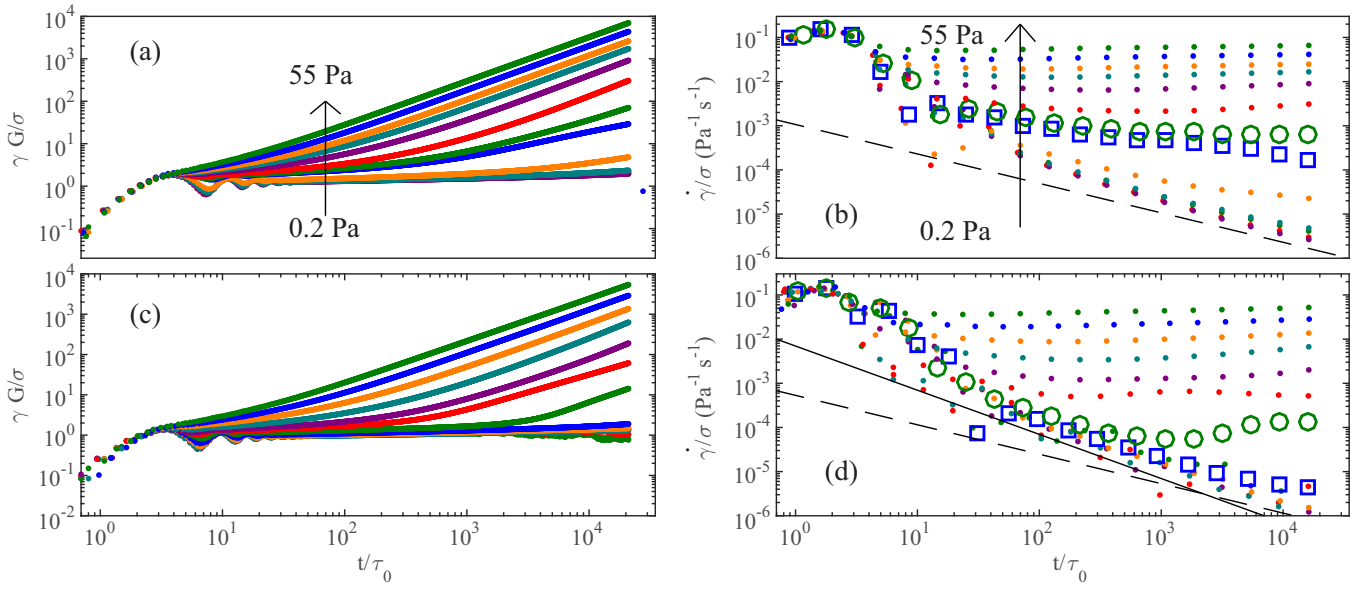

FIG. 2. (a) Normalized deformation $\gamma\sigma/G$ versus time t for $\sigma = 0.2$ to 55 Pa for a young ($t_w = 300$ s) $\phi = 0.64$, $R = 300$ nm sample. (b) Corresponding shear rates over stress, $\dot{\gamma}/\sigma$, versus time with the dash line indicating the power law $-2/3$. (c) Normalized deformation $\gamma\sigma/G$ versus time t for the same sample and conditions with (a) for an aged sample($t_w = 10^5$ s). (d) $\dot{\gamma}/\sigma$ versus time corresponding to measurements in (c). The dash line indicates power law exponent of $-2/3$ and the solid line, linear decrease. In both (b) and (d) the large squares and circles represent stresses just below and above the yield stress, respectively.

light captured on a multipixel detector (CCD camera) and analyzed them using the time-resolved correlation (TRC) technique [48]. As the sample is quite turbid but not in the diffusive wave spectroscopy (DWS) regime, any unscattered or singly scattered light is removed in transmission by placing the sample between crossed polarizers as in Ref. [49]. Under such conditions, the dynamics probed are related with particle motions at length scales roughly equal to the cage size, or the interparticle distance. TRC provides the normalized two-time autocorrelation function, $c_I(t,\tau) = \langle I(p,t)I(p,t+\tau)\rangle_p / \langle I(p,t)\rangle_p^2$ of the pixel intensity, $I(p,t)$, between an image at a time t and $t+\tau$, effectively replacing time averaging with pixel averaging. For a given t we can construct the intensity autocorrelation function $g_2(\tau) - 1$ by taking the time average of $c_I(t,\tau)$ around t. Fitting $g_2(\tau) - 1$ by a stretched or compressed exponential we determine the relaxation time, τ_f, as a function of the age of the sample, t_w.

III. RESULTS

A. Constant stress experiments short-time creep

In Fig. 2, we present $\gamma(t)$, normalized by σ/G (with G the elastic modulus determined by linear rheology at 1 Hz) for a $\phi = 0.64$, $R = 300$ nm, hard-sphere glass submitted to a range of constant stresses below and above the yield stress, σ_y (= 18 Pa). The experiments were carried out both with a freshly rejuvenated (young, $t_w = 300$ s) sample as well as an aged one at zero stress for $t_w = 10^5$ s. Similar to previous experiments [25,33,50] and theoretical predictions [29,51], when the applied stress is above the yield stress a short elastic deformation is followed by flow at constant viscosity, whereas below the yield stress, a creeping flow is detected with the viscosity continuously increasing with time. The initial elastic strain increase is followed by strain oscillations due to coupling of the sample viscoelastic properties with the tool inertia [33,50]. The subsequent creeping regime, for stresses below and near the yield stress, is caused by a combination of local stress relaxation and shear induced deformation of local cage structures. While both young and aged samples behave similarly for $\sigma \ll \sigma_y$ and $\sigma \gg \sigma_y$ when stresses around the yield stress are applied the response is quite different. At $\sigma \geqslant \sigma_y$, the steady state takes longer to reach for an aged sample compared to a young one. In the aged sample and for $\sigma \leqslant \sigma_y$ the shear rate, $\dot{\gamma}$, decreases (or the viscosity, η, increases) linearly with time exhibiting a logarithmic creep reminiscent of granular systems near jamming [52], and correspond to what is observed in numerical studies [29,51]. For the young sample though the behavior follows a power law close to an Andrade creeping law, with $\dot{\gamma} \propto t^{-n}$ (or $\eta \propto t^n$) and $n \simeq 0.7$, which is within experimental error of 2/3, the value expected for Andrade creep [53], often observed in polycrystalline metals [54]. A transition from Andrade to logarithmic creep was similarly observed in glasses of softer core-shell microgels near close packing with a diverging transition timescale as the yield stress is approached from below [25]. This is, however, different to what is found by Chaudhuri and Horbach [32], where an exponent $\dot{\gamma} \propto t^{-3/4}$ was observed independently of time. This difference may be related to the different protocols to rejuvenate the sample, high temperature numerically and high shear experimentally.

B. Frequency sweep and superposition rheometry

We now turn to the effect of aging on the linear viscoelastic properties of our system measuring the temporal evolution of G' and G'' at rest or under external stress. For the latter we performed parallel superposition rheometry experiments

where a small oscillatory stress, with amplitude σ_2 and angular frequency ω, is superimposed on a constant shear stress σ_1. The total applied stress is $\sigma = \sigma_1 + \sigma_2 \cos(\omega t)$ with σ_2 small enough to be considered as a linear perturbation [$\sigma_2 + \sigma_1 < \sigma_y$ and $\sigma_2 \ll G'(\omega)$]. Under such conditions the resulting shear rate is of the form $\dot{\gamma} = \dot{\gamma}_1 + \dot{\gamma}_2 \cos(\omega t + \delta)$, where δ is the phase difference between stress and strain, while $\sigma_1(\dot{\gamma}_1)$ is expected to reproduce the steady shear flow curve. For $\sigma_1 < \sigma_y$, the sample is creeping, as discussed above, with $\dot{\gamma}_1$ approaching zero with increasing time, as the sample ages under stress. To ensure that the system remains in the creeping regime, we use $\sigma_1 + \sigma_2 < \sigma_y$ with σ_2 always in the linear regime (even for $\sigma_1 = 0$). During such tests, the equivalent linear viscoelastic moduli are

$$G' = \frac{\omega\sigma_2 \sin(\delta)}{\dot{\gamma}_2}, \tag{1}$$

$$G'' = \frac{\omega\sigma_2 \cos(\delta)}{\dot{\gamma}_2}. \tag{2}$$

As it has been pointed out before [55], in order to acquire meaningful G' and G'' in such parallel superposition experiments the frequency of the probing σ_2 has to be much higher than the steady shear rate due to σ_1. Here the steady shear rate measured is always many orders of magnitude smaller than the applied probe frequency ω, and therefore the extracted G' and G'' represent, to a good approximation, the viscoelastic spectra of the system under shear. A better approach would be to superimpose a small amplitude (linear) oscillatory shear measurement orthogonal to steady stress (nonlinear) creep test. However, although such an approach has been successfully used to probe the convective cage release in similar colloidal glasses under steady-rate experiments [56], it requires the use of a specialized rheometer and cannot be performed under constant stress or combined with the light-scattering probes used here.

Figure 3 shows the time evolution of G' and G'' after shear rejuvenation (see Sec. II B) for two different concentrations ($\phi = 0.6$ and 0.62) at $\sigma_1 = 0$ (rest) and $\sigma_1 = \sigma_y/3$ (under stress). In all cases G' and G'' exhibit a very weak decrease (G' drops by about 3%) during the first minutes and then remain nearly constant with time. Moreover, experiments both at rest ($\sigma_1 = 0$) and under constant weak stress ($\sigma_1 = \sigma_y/3$) give similar values of G' and G'', indicating the lack of significant thixotropy under such shear history in the present nearly hard-sphere glasses, in agreement with previous findings in similar colloidal glasses and shear induced crystals [39]. We can relate the early time decrease of G' in our experiments with the initial increase of τ_f observed with TRC (presented below), both alluding to fast structural rearrangements in the sample immediately after shear rejuvenation ends. Our superposed oscillatory rheometry probe [with $\sigma_2 \cos(\omega t)$], however, does not pick up (in G' and G'') any indications of the long time fluctuations observed in the steady stress, creep experiments (with $\sigma_1 = \sigma_y/3$) in the measured shear rate (see Fig. 4), or in the internal dynamics probed by light scattering (see Fig. 5). Since the probing oscillatory frequency ω for σ_2 is large compared to the maximum shear rate ($\dot{\gamma}_1 \simeq 10^{-5}$ s^{-1}) acquired under σ_1, such long-time thermal fluctuations are nearly invisible in the superposition experiments.

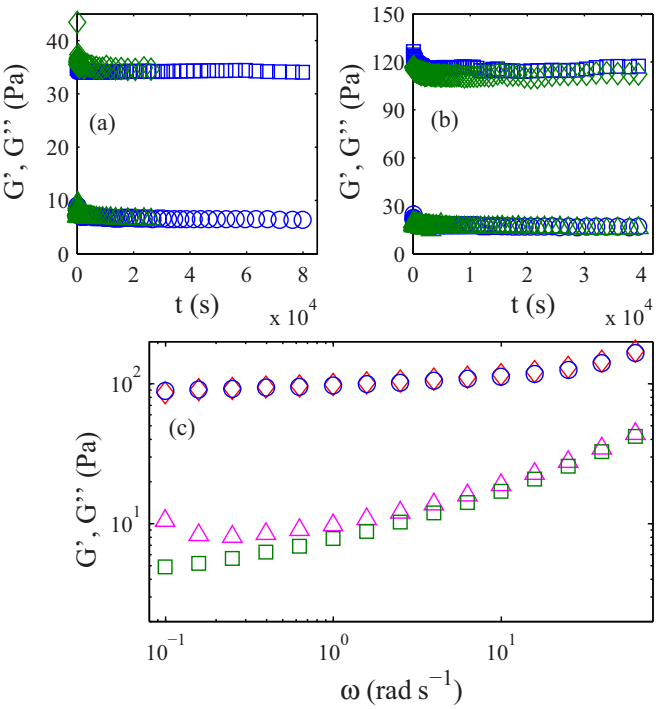

FIG. 3. (a) G' and G'' versus time t, for a $\phi = 0.6$, $R = 138$ nm suspension with $\sigma_1 = 0.3$ Pa (G' □, G'' ○) and a $\sigma_1 = 0$ (G' ◇, G'' △) during superposition experiment at $\omega = 2\pi$ rad/s. (b) G' and G'' versus time t, for a $\phi = 0.62$, $R = 138$ nm suspension with $\sigma_1 = 1$ Pa (resp., □, ○) and a $\sigma_1 = 0$ (resp., ◇, △) during superposition experiment at $\omega = 2\pi$ rad/s. (c) Frequency sweep for a rejuvenated [G' (○), G'' (△)] and an aged sample $t_w = 31000$ s [G' (◇), G'' (□)] at $\phi = 0.62$, $R = 138$ nm.

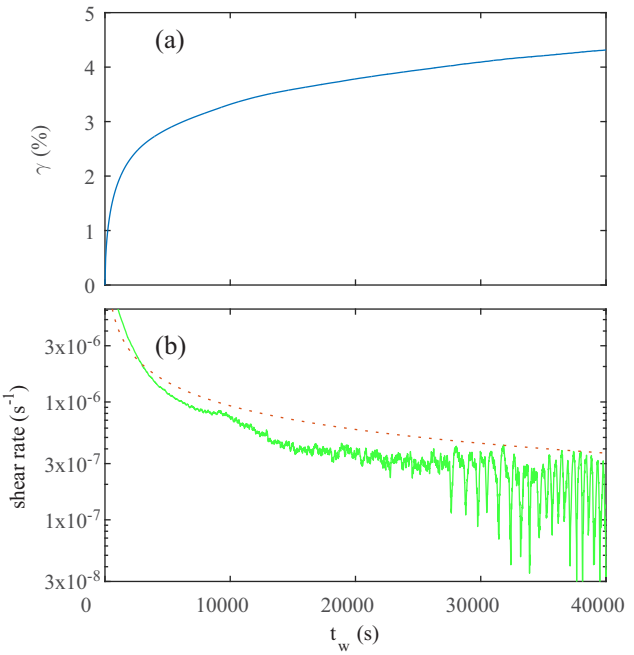

FIG. 4. (a) Strain versus time for a $\phi = 0.62$, $R = 138$ nm sample with $\sigma = 1$ Pa. (b) Corresponding shear rate (continuous line) versus time, the dotted line shows a $-2/3$ power law.

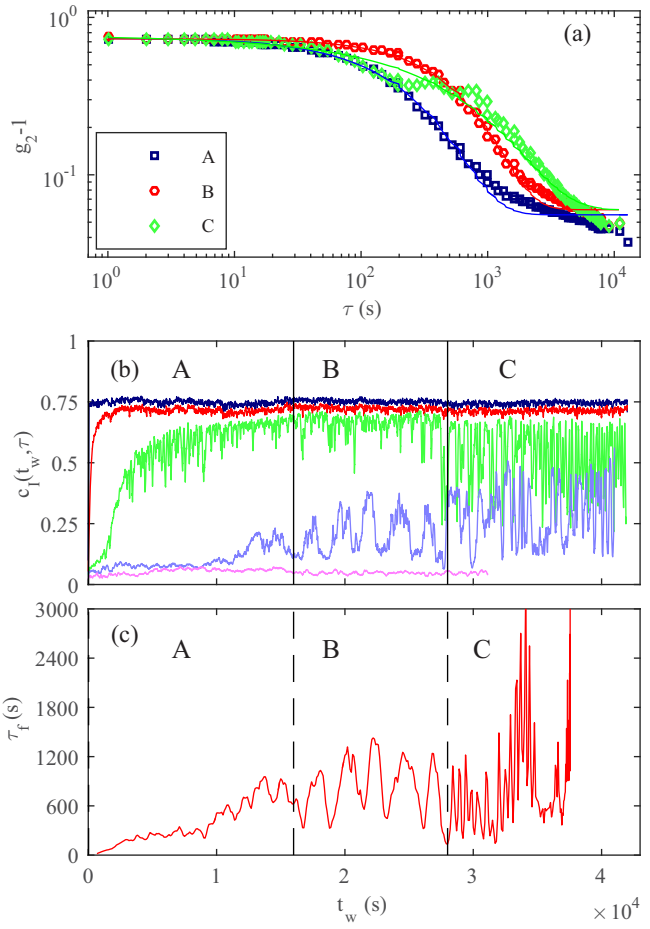

FIG. 5. Dynamic light-scattering experiments during a long creep experiment at $\sigma = 1$ Pa (for $\phi = 0.62$, $R = 138$ nm). (a) $g_2(\tau) - 1$ averaged over each subregime, the continuous lines are the best fit by a stretched exponential. (b) c_1 versus waiting time t_w for $\tau = 1$ s (dark blue), $\tau = 10$ s (red), $\tau = 105$ s (light green), $\tau = 1000$ s (cyan), and $\tau = 10887$ s (pink). Vertical black lines separate the three regimes. (c) Relaxation time τ_f versus waiting time, t_w.

Figure 3(c) shows the linear viscoelastic spectrum of a young and an aged sample. G' is almost unaffected by aging at all frequencies, whereas at low frequencies, G'' decreases weakly in the aged sample. In concentrated hard-sphere systems the elastic energy, of entropic character, stored in a cage may be dissipated at low frequencies through out-of-cage particle motions. Thus, the low-frequency increase detected in G'', indicative of a peak at lower ω that is outside the experimental window, is linked to the long-time α-type relaxation process. As the system ages, the α relaxation slows down [9,12], causing a decrease of G'' as its maximum shifts to lower ω. On the other hand, the high-frequency response is related with shorter timescales and more local in-cage motions that are not affected by aging. Therefore, G'' remains constant at high frequencies but decreases at low frequencies, similarly with findings in soft colloidal glasses [17]. This behavior indicates that the time between long range (and slow) rearrangement events increases in agreement with the argumentation used in soft glassy rheology (SGR) [28,29] to explain the increase of the apparent viscosity with time as the frequency of local rearrangements, enabling slow creep, decreases. In this way the sample under constant stress (σ_1) is progressively slowing down (with $\dot{\gamma}_1$ tending to zero) as it evolves into deeper local energy minima of the energy landscape. The related slowing down of the intrinsic long-time relaxation as the system ages is captured by the relaxation time extracted from dynamic light-scattering experiments under shear shown in Fig. 5 and discussed below.

The small initial decrease of the elastic modulus is somewhat more surprising than the low-frequency decrease of G''. Aging studies in different systems, such as colloidal suspensions and glasses of repulsive or nearly hard-sphere particles [17,38,39], show a logarithmic or weak power-law increase of G' with waiting time. On the other hand, systems with attractive interactions such as depletion gels [57–59] and various soft pastes (consumer products or industrial systems) [50] may exhibit stronger increase of G' with time. A common feature of the latter is the existence of weak or strong attractions that cause a nonergodic transition at volume fractions smaller than that of hard spheres and invoke thixotropic phenomena related with aggregation, network formation, and global structural reorganization.

In some systems of nearly hard or soft repulsive particles (such as in Refs. [17,38]) with similar flow curves and dynamic frequency sweeps to the ones obtained here, the evolution of their viscoelastic properties were only measurable at long times (equivalent to ten of thousands of Brownian times); however, G' was slowly increasing with time, in contrast to findings here where G' exhibits an initial fast decrease toward a constant value that persists to long times. Earlier experiments in a similar nearly HS glasses and shear-induced crystal (PMMA particles in octadecene; but at higher ϕ than here) are largely in agreement with our current findings as they showed only a very weak (if not at all) increase in G' for times 10^3 s after shear rejuvenation [39]. Although not significant, the different time evolution of G' in the present system of PMMA HS particles and that of silica particles [38] or soft jammed microgels [17] could be attributed to the different interaction potential, with microgels and charged stabilized silica expected to have longer range repulsions. Moreover, ultrasoft, interpenetrating multiarm star polymers exhibit an even stronger and two-step evolution of G' while attractive particle suspensions forming gels (as those studied in Ref. [57]) exhibit stronger increase of G' related with the build-up and coarsening of their microstructure [58,59].

It should be noted that the time evolution of G' after shear rejuvenation with a decrease at short times and a subsequent almost constant value for longer times is reminiscent of highly confined systems, such as onion phases [60] or cross-linked actin filaments [61], where relaxation of stored stresses following a rapid quench also results in a short-time decrease of G'. Therefore, here the decrease of G' may be due to the relaxation of such internal stresses following a rapid transition from shear melted (rejuvenated) state back to the glassy solid-like state after shear cessation. Partial relaxation of frozen-in stresses after shear rejuvenation have been reported recently in similar hard-sphere glasses to depend on the shear rate applied prior to shear cessation [44]. Local stresses resulting from loading and/or preshear can be stored through cage deformation. As stresses are relaxed cages becomes more

homogeneous hence increasing the free space of particles. This increase in free space ultimately leads toward a decrease of the elastic modulus. This can be understood as local rearrangement of neighboring particles similar to what is observed in low polydispersity samples where shear-induced crystallization of a glass sample leads to a drop of G' [39].

C. Long-time creep and light-scattering experiments

To acquire a more complete picture of aging under constant stress, we extended the creep measurements to longer times, reaching up to several days and performed simultaneous dynamic light-scattering measurements to probe the internal dynamics as a function of time.

In Fig. 4(a), we show the strain evolution during a long creep test for a $\phi = 0.62$, $R = 138$ nm hard-sphere glass under $\sigma = 1$ Pa. The applied stress is a third of the yield stress obtained from fitting of the flow curve. The strain increases with time following, at long times, a power-law creep response with an exponent close to 1/3, as seen by the power-law decrease of the shear rate [Fig. 4(b)]. The latter progressively decreases with time, t_w, reaching very low values ($10^{-7}\mathrm{s}^{-1}$, near instrumental limits) and indicating an apparent halt of shear deformation. Moreover, at long times the shear rate exhibits strong fluctuations [Fig. 4(b)], which are often accompanied by sudden intermittent jumps in the strain.

The microscopic dynamics during such long creep measurements ($\sigma = 1$ Pa) were probed by dynamic light scattering. In Fig. 5, we present results from such simultaneous dynamic light-scattering experiments on the sheared sample, revealing three regimes. Figure 5 shows the intensity autocorrelation function, $g_2(\tau) - 1$, at three different aging times, indicating a progressive slowing down with time of the internal relaxation of the system under shear (averaged over the corresponding time period). We can investigate in more detail the time evolution of the dynamics by looking at c_I [Fig. 5(b)] and the relaxation time τ_f [Fig. 5(c)] deduced from $g_2(\tau)$. Three regimes are identified: in the first one (regime A) a continuous increase of the relaxation time, τ_f, is observed for about 4 h. This behavior is often observed in concentrated soft matter systems following rejuvenation [48], and corresponds, on a macroscopic scale, to the initial fast increase of the apparent viscosity. At a latter stage, in the second regime (regime B) the relaxation time, τ_f, exhibits some fluctuations around an average time of about 1000 s. These fluctuations have a frequency similar to the relaxation time. Finally, in the third regime (regime C), the system exhibits significantly stronger fluctuations of the internal relaxation time, which are accompanied by strong fluctuations in the shear rate measured by the rheometer [Fig. 4(b)].

The fluctuations of the average relaxation time under shear are also linked with strong intermittency observed in the two-point correlation function that reflects pronounced shear-induced dynamic heterogeneities in the sample. Similar prolonged creep that leads to an almost ideal solid-like response with a strain plateau (a halt of flow and deformation) has been seen in soft multiarm stars [33] and soft industrial pastes [50], while shorter creep measurements in soft core-shell microgels did not reach such state [25,31]. Whereas in the case of soft multiarm stars [33] the glassy state under $\sigma \leqslant \sigma_y$ reaches an almost perfect strain plateau after a prolonged creep, for hard-sphere glasses such plateau is often interrupted by sudden strain jumps occurring randomly in time and followed by a subsequent progression to a new strain plateau. These strain jumps are linked with fluctuations of temperature gradients, suggesting some kind of externally triggered local stress or deformation fields that cannot relax sufficiently (as in the case of the ultrasoft multiarm stars) and hence can propagate like avalanches throughout the sample, partly rejuvenating it.

Some of the decorrelation events observed are partially reversible as can be deduced from the shape of the events measured in the $c_I(t_w,\tau)$ (see also Ref. [62]). In such concentrated colloidal suspensions with slow internal relaxations an irreversible event corresponds to faster configurational (microstructural) changes in the sample occurring on timescales shorter than the average relaxation time τ_f. In response the scattered light intensity is decorrelated between images taken before and after the time of the event, t_{event}, and $c_I(t_w,\tau)$ grows back to pre-event values when both correlated images are taken at times greater than t_{event}. As a result $c_I(t_w,\tau)$ exhibits drops of correlation of duration $\simeq\tau$ [62]. This leads to monotonically decreasing $g_2(\tau) - 1$. On the other hand, if the events are partially reversible, $c_I(t_w,\tau)$ with τ larger than the characteristic time of the reversible events, should decrease and then increase on a duration smaller than τ as the system goes back to a previous configuration. Consequently, for irreversible events at every time t_w, $g_2(\tau)$ should decay monotonously, whereas reversible events lead to a non-monotonous, oscillating, $g_2(\tau)$.

In our case, the oscillations observed in regime B [see Figs. 5(a) and 5(b)] clearly correspond to irreversible rearrangements in the sample; typically, $c_I(t_w,\tau)$ presents drops of correlation of length τ and $g_2(\tau) - 1$ averaged on this time window decreases monotonically. On the contrary, the fast oscillations observed in the third regime are partially reversible as the oscillations of c_I seem to be correlated with the oscillations in the shear rate; this can also be seen in $g_2(\tau) - 1$ that presents a short plateau for $200 < \tau < 1000$ s, which corresponds to the fast reversible events observed in regime C.

Since both the integrated strain rate (and therefore the total strain) and c_I (from which $g_2(\tau)$ and τ_f are deduced) present the same overall time response we should be able to directly compare and correlate them. One method would be to directly compare the strain difference between times t_w and $t_w + \tau$ with $c_I(t_w,\tau)$. However, this does not yield a clear correlation as fluctuations of γ are too small. Therefore, we first need to magnify the small fluctuations observed in the shear strain. To verify the relation between the fluctuations observed in strain γ and in the measured relaxation time τ_f, we first isolate the high frequency oscillations in $\gamma(t_w)$ by removing an average of γ over 1000s: $\gamma_{fl} = \gamma(t_w) - <\gamma>_{1000}$.

To directly compare these oscillations with c_I we calculate the strain decorrelation function:

$$\psi(t_w,\tau) = \exp\left(-\frac{\Delta\gamma^2}{\gamma_0}\right) \tag{3}$$

$$\Delta\gamma = \gamma(t_w+\tau) - \gamma(t_w) + \alpha[\gamma_{fl}(t_w+\tau) - \gamma_{fl}(t_w)], \tag{4}$$

where γ_0 is a multiplication constant needed for ψ to reproduce the behavior of c_I, while α is a weight that shows how important the low frequencies fluctuations are compared to the average trend. Therefore, γ_0 is dependent on the optical setup and the optical properties of the sample. On the other hand, α indicates how much the response deviates from a linear dependency of the correlation with strain. For a purely elastic sample with small deformations we would expect $\alpha \simeq 1$, whereas a large α indicates nonlinearity caused by rearrangements in the sample. This simple phenomenological expression describes how much the system is deformed between t_w and $t_w + \tau$, but the role of high frequency deformation in the decorrelation process is amplified through the α coefficient; in our case $\alpha \simeq 15$. By choosing the same τ for both c_I and ψ, we directly compare the decorrelation in the scattered intensity and the displacement.

In Fig. 6(a), we present together c_I and ψ in regime A for $\tau = 273$ s, and $\alpha = 15$, which was chosen to optimize the visual similarity between c_I and ψ at this τ. As can be seen, both functions present an overall increase with time that corresponds to the slowing down of the suspensions, and drops at the same t_w. Similarly, Fig. 6(b) shows c_I and ψ in regime B for $\tau = 1000$ s, and $\alpha = 15$, both functions have no overall trend but present fluctuations, which are stronger when they happen at the same time. Fluctuations in c_I have roughly a square shape and a constant duration $\simeq\tau$, while the corresponding drops in ψ have no fixed shape. Finally, Fig. 6(c) presents c_I and ψ in regime C for $\tau = 442$ s, and $\alpha = 15$. Again, both curves exhibit fluctuations that are fully correlated in time; moreover, here both curves are clearly similar, with very close amplitudes of ψ and c_I fluctuations.

Fluctuations in shear rate and thus strain deformation may propagate in the sample causing intermittent local microstructural rearrangements that decorrelate the scattering intensity. Thus, small fluctuations in externally imposed deformation, and thus in ψ, may show up amplified in c_I. Both fluctuations may also be related or even caused by external mechanical vibrations and temperature variations.

In the third subregime (C), oscillations in c_I take place simultaneously with the small oscillations in γ as evidenced in Fig. 6(c) by the fully correlated time evolution of ψ and c_I. Rheological measurements in this regime reveal a succession of regimes with almost no displacement (strain deformation coming to a halt) followed by weak shear, reminiscent of a stick-slip response. To find the cause of these oscillations, similar experiments were performed under zero shear rate and zero stress conditions. In both cases small variations in the strain were observed with comparable period. This suggests that small external mechanical vibrations present in the environment may trigger stress fluctuations in the sample itself. Indeed, because of the extreme sensitivity of our measurements under weak stresses, small displacements of the top plate (few nm) may result in measurable fluctuations of the acquired light scattering intensity and c_I leading to a decorrelation in $g_2(\tau)$.

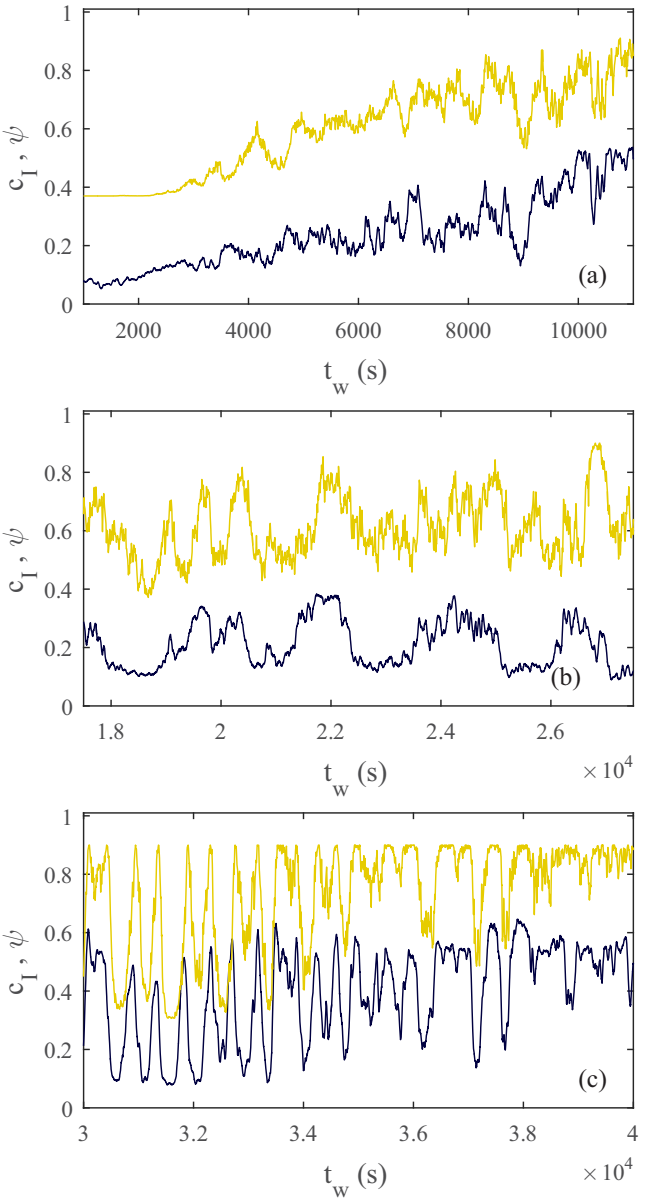

FIG. 6. Correlations in scattered intensity and deformation: (a) ψ [yellow (light gray)] and c_I (dark blue) versus waiting time t_w in regime A for $\tau = 273$ s, with $\gamma_0 = 0.03$. (b) ψ [yellow (light gray)] and c_I (dark blue) versus waiting time t_w in regime B for $\tau = 1000$ s, with $\gamma_0 = 0.04$. (c) ψ [yellow (light gray)] and c_I (dark blue) versus waiting time t_w in regime C for $\tau = 442$ s, with $\gamma_0 = 0.035$. In (a), (b), and (c) we plot $\psi + 0.3$ for better visibility. The suspension is at $\phi = 0.62$, $R = 138$ nm.

D. Stress-reversal experiments

A possible microscopic mechanism responsible for the prolonged creep and slow decrease of the shear rate with time toward a halt of strain deformation (for $\sigma \leqslant \sigma_y$) is shear-induced jamming detected both in colloidal [63] and athermal systems [64]. In the case of jamming under low shear stresses, we expect the creation of a network of force chains that would percolate in the direction of shear. These could be very sensitive to temperature fluctuations and hence could cause the strong fluctuations observed in $c_I(t_w, \tau)$. To test such a scenario, we perform successive creep and recovery experiments, where the stress is applied first in one direction and subsequently in the opposite one. Figure 7(a) depicts

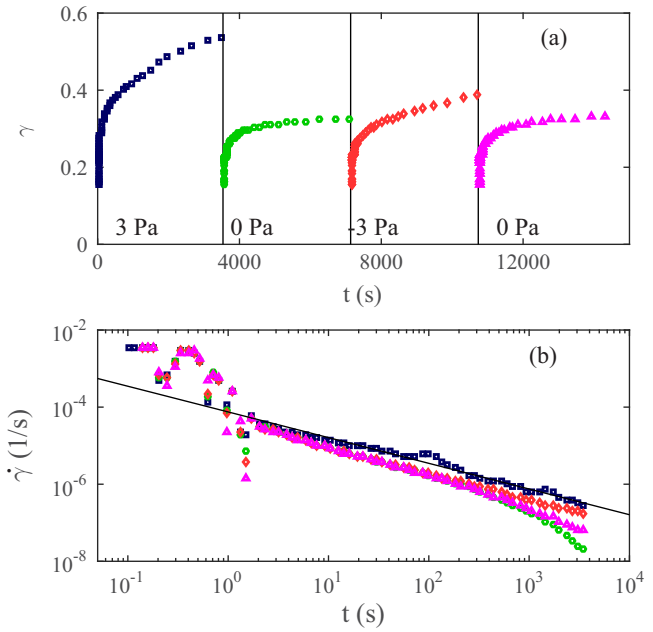

FIG. 7. Stress reversal experiments: (a) Strain versus time for a constant stress of 3 Pa (creep test □) followed by a constant stress 0 Pa (recovery test ○) then a constant stress of −3 Pa (reverse creep test ◇) and finally a constant stress of 0 Pa (recovery test △). (b) Log-log representation of the corresponding shear rates versus time for a PMMA HS glass (particles with $R = 138$ nm) at $\phi = 0.65$ in octadecene. The continuous line indicates a power-law exponent $-2/3$.

the strain attained during such a test in one direction at $\sigma = \sigma_y/3 = 3$ Pa and then in the opposite direction with $\sigma = -3$ Pa for a sample at $\phi = 0.65$, $R = 138$ nm. Between the two creep experiments a recovery test was introduced ($\sigma = 0$) during which the strain is partly recovered due to the elastic recoil of the deformed cage as in Ref. [20].

A shear induced jamming is expected to create a fragile network [65,66] and a stress reversal would then cause unjamming (or rejuvenation) due to unlocking of jammed regions leading to an enhancement (or speed up) of creep (or flow) upon stress reversal. After such unjamming the sample would reach a state similar to its initial unsheared one, which would then follow the same creeping response in the opposite direction. However, here, after the stress was reversed, we detect a weaker strain increase than what was originally measured in the forward direction [Fig. 7(a)]. Figure 7(b) shows the resulting shear rate under stress ($\sigma = \pm 3$ Pa) and during relaxation ($\sigma = 0$ Pa). The shear rate evolution with time under constant stress in both directions is decreasing following reasonably well the power-law behavior as $t^{-2/3}$ for rejuvenated samples. However, the shear rate for the reversed negative stress is below the one for the initial deformation under positive stress. Therefore, reverting the stress does not result in rejuvenation or unjamming of the sample, but rather keeps on aging from the previous, aged state. Hence, jamming is not responsible for the weak strain increase that, after a prolonged creep, leads to an almost constant strain plateau (deformation halt). On the other hand, during relaxation ($\sigma = 0$ Pa) the shear rate drops at long-times faster than the power law followed under constant stress; as a result, the deformation eventually stops and strain is not entirely recovered in agreement with earlier creep and recovery experiments [20].

Alternatively, such a response may relate with local plastic events involving cooperative rearrangements and microscopic stress relaxation, which are caused by an external weak shear stress (below the yield stress), and thus low strain rates, that would not fully or partially rejuvenate the sample, and lead the system in deeper local minimum of the energy landscape. Such a process of aging under shear is only temporarily interrupted when the stress is removed; then partial strain recovery reflects the relaxation of a mildly deformed cage microstructure. Subsequently, upon stress reversal (with the same low magnitude stress) the process may continue with the system being at an aged state similar to that before stress removal. However, we do not have any indication of over-aging under shear like the effects detected in Ref. [13]. The above findings and interpretation bares resemblance with the basic features of elastoplastic models for yield stress fluids [21,67–70], although direct comparison is not possible as here experiments are conducted under constant stress and not shear rate, which results in widely different response in the out-of-equilibrium regime. Recent calculations realized at constant stress [51] using a kinetic Monte Carlo algorithm show similar power-law dependency of the strain with time, though no time dependence of the exponent was observed.

IV. CONCLUSIONS

In this work, we used a range of experimental techniques to study the creep behavior of colloidal nearly hard-sphere glasses. Our experiments partially reproduce the numerical results obtained in Ref. [29], where applying a constant stress below the yield stress results in a prolonged creep flow. Local rearrangements under stress lead to such response with an apparent viscosity, which diverges with waiting time as the strain approaches a constant value plateau (or increases logarithmically); therefore, the viscosity measured in the early stage clearly has an out-of-equilibrium character. Microscopically, the sample reaches a more stable, although still amorphous, configuration related to a lower energy minimum. Comparing the creep flow of young and aged samples reveals an important difference between experiments and theoretical (or simulation) approaches. In the later, the system starts from a well-equilibrated state and is driven to a deeper glassy state by application of a constant stress with the shear rate decreasing as t^{-1} similarly to what is observed experimentally in aged samples. However, shear rejuvenated samples start off in a configuration with strong internal stresses created either by loading or rejuvenation at high shear rate. In such cases, aging is governed by relaxation of the stored stresses rather than an over-aging driven by shear. As a result, we find a β-creep response for young samples. Interestingly, the increase of viscosity with time under stress contrasts with what is observed in monodisperse HS glasses [39], where an oscillatory shear can induce crystallization and decrease the apparent viscosity of the system.

We showed that, for model nearly hard spheres, aging is accompanied by a weak initial decrease of the elastic and loss modulus. This decrease is related to the relaxation of partly

frozen-in stresses resulting from shear rejuvenation. Beyond this point, a continuous decrease of localized events is taking place in the sample as it ages under stress leading, after a relatively prolonged logarithmic creep, to an almost ideal strain plateau, yet with intermittent externally triggered avalanche-type events. This is further confirmed by TRC experiments under stress. These experiments show that the creep is directly related to the internal relaxation time of the sample, reflecting a succession of events in the sample.

ACKNOWLEDGMENTS

We thank A. B. Schofield for the synthesis of the PMMA particles and N. Koumakis for fruitful discussions. We acknowledge EU funding through EU FP7-Infrastructures "ESMI" (Grant No. CP&CSA-2010-262348). We also acknowledge funding from the Greek Ministry of Education, Lifelong Learning and Religious Affairs through research funding program "Thales" (project "COVISCO" Grant No. 380238) and Aristeia II (project "MicroSoft" Grant No. 3144).

[1] D. Bonn, J. Paredes, M. M. Denn, L. Berthier, T. Divoux, and S. Manneville, arXiv:1502.05281 (2015).
[2] P. N. Pusey, *Liquids, Freezing and the Glass Transition* (North Holland, Amsterdam, 1991).
[3] L. Cipelletti and L. Ramos, J. Phys.: Condens. Matter **17**, R253 (2005).
[4] W. C. K. Poon, J. Phys.: Condens. Matter **14**, R859 (2002).
[5] K. N. Pham, A. M. Puertas, J. Bergenholtz, S. U. Egelhaaf, A. Moussaïd, P. N. Pusey, A. B. Schofield, M. E. Cates, M. Fuchs, and W. C. K. Poon, Science **296**, 104 (2002).
[6] P. Coussot, Soft Matter **3**, 528 (2007).
[7] S. A. Rogers, P. T. Callaghan, G. Petekidis, and D. Vlassopoulos, J. Rheol. **54**, 133 (2010).
[8] Y. M. Joshi and G. R. K. Reddy, Phys. Rev. E **77**, 021501 (2008).
[9] D. El Masri, G. Brambilla, M. Pierno, G. Petekidis, A. B. Schofield, L. Berthier, and L. Cipelletti, J. Stat. Mech. (2009) P07015.
[10] D. El Masri, L. Berthier, and L. Cipelletti, Phys. Rev. E **82**, 031503 (2010).
[11] X. Di, K. Z. Win, G. B. McKenna, T. Narita, F. Lequeux, S. R. Pullela, and Z. Cheng, Phys. Rev. Lett. **106**, 095701 (2011).
[12] V. A. Martinez, G. Bryant, and W. van Megen, J. Chem. Phys. **133**, 114906 (2010).
[13] V. Viasnoff, S. Jurine, and F. Lequeux, Faraday Discuss. **123**, 253 (2003).
[14] R. Di Leonardo, F. Ianni, and G. Ruocco, Phys. Rev. E **71**, 011505 (2005).
[15] L. Djaoui and J. Crassous, Granular Matter **7**, 185 (2005).
[16] S. Kaloun, M. Skouri, A. Knaebel, J. P. Munch, and P. Hebraud, Phys. Rev. E **72**, 011401 (2005).
[17] E. H. Purnomo, D. van den Ende, J. Mellema, and F. Mugele, Phys. Rev. E **76**, 021404 (2007).
[18] A. S. Negi and C. O. Osuji, Phys. Rev. E **82**, 031404 (2010).
[19] P. Hébraud and F. Lequeux, Phys. Rev. Lett. **81**, 2934 (1998).
[20] G. Petekidis, D. Vlassopoulos, and P. N. Pusey, J. Phys.: Condens. Matter **16**, S3955 (2004).
[21] G. Picard, A. Ajdari, F. Lequeux, and L. Bocquet, Phys. Rev. E **71**, 010501 (2005).
[22] P. Coussot, H. T. Huynh, Q. D. Nguyen, and D. Bonn, J. Rheol. **46**, 573 (2002).
[23] K. N. Pham, G. Petekidis, D. Vlassopoulos, S. U. Egelhaaf, W. C. K. Poon, and P. N. Pusey, J. Rheol. **52**, 649 (2008).
[24] T. Divoux, D. Tamarii, C. Barentin, S. Teitel, and S. Manneville, Soft Matter **8**, 4151 (2012).
[25] M. Siebenbürger, M. Ballauff, and T. Voigtmann, Phys. Rev. Lett. **108**, 255701 (2012).
[26] M. Leocmach, C. Perge, T. Divoux, and S. Manneville, Phys. Rev. Lett. **113**, 038303 (2014).
[27] T. Sentjabrskaja, P. Chaudhuri, M. Hermes, W. C. K. Poon, J. Horbach, S. U. Egelhaaf, and M. Laurati, Sci. Rep. **5**, 11884 (2015).
[28] S. M. Fielding, P. Sollich, and M. E. Cates, J. Rheol. **44**, 323 (2000).
[29] S. M. Fielding, M. E. Cates, and P. Sollich, Soft Matter **5**, 2378 (2009).
[30] E. Agoritsas, E. Bertin, K. Martens, and J.-L. Barrat, Eur. Phys. J. E **38**, 71 (2015).
[31] V. Carrier and G. Petekidis, J. Rheol. **53**, 245 (2009).
[32] P. Chaudhuri and J. Horbach, Phys. Rev. E **88**, 040301(R) (2013).
[33] C. Christopoulou, G. Petekidis, B. Erwin, M. Cloitre, and D. Vlassopoulos, Philos. Trans. R. Soc. London A **367**, 5051 (2009).
[34] I. W. Chen and A. S. Argon, Acta Metall. **27**, 749 (1979).
[35] P. Schall, D. A. Weitz, and F. Spaepen, Science **318**, 1895 (2007).
[36] C. Liu, E. E. Ferrero, F. Puosi, J.-L. Barrat, and K. Martens, Phys. Rev. Lett. **116**, 065501 (2016).
[37] G. Picard, A. Ajdari, F. Lequeux, and L. Bocquet, Eur. Phys. J. E **15**, 371 (2004).
[38] C. Derec, G. Ducouret, A. Ajdari, and F. Lequeux, Phys. Rev. E **67**, 061403 (2003).
[39] N. Koumakis, A. B. Schofield, and G. Petekidis, Soft Matter **4**, 2008 (2008).
[40] D. Bonn, S. Tanase, B. Abou, H. Tanaka, and J. Meunier, Phys. Rev. Lett. **89**, 015701 (2002).
[41] G. Bryant, S. R. Williams, Q. LinMao, I. K. Snook, E. Perez, and F. Pincet, Phys. Rev. E **66**, 060501(R) (2002).
[42] D. B. Hough and L. R. White, Adv. Colloid Interface Sci. **14**, 3 (1980).
[43] B. Lee and S. Komarneni, eds., *Processing of Ceramics, Second Edition* (CRC Press, Boca raton, FL, 2005).
[44] M. Ballauff, J. M. Brader, S. U. Egelhaaf, M. Fuchs, J. Horbach, N. Koumakis, M. Krüger, M. Laurati, K. J. Mutch, G. Petekidis, M. Siebenbürger, T. Voigtmann, and J. Zausch, Phys. Rev. Lett. **110**, 215701 (2013).
[45] G. Petekidis, D. Vlassopoulos, and P. N. Pusey, Faraday Discuss. **123**, 287 (2003).
[46] P. Olsson and S. Teitel, Phys. Rev. Lett. **99**, 178001 (2007).
[47] F. Puosi, J. Olivier, and K. Martens, Soft Matter **11**, 7639 (2015).
[48] L. Cipelletti, H. Bissig, V. Trappe, P. Ballesta, and S. Mazoyer, J. Phys.: Condens. Matter **15**, S257 (2003).

[49] G. Petekidis, A. Moussaid, and P. N. Pusey, Phys. Rev. E **66**, 051402 (2002).
[50] P. Coussot, H. Tabuteau, X. Chateau, L. Tocquer, and G. Ovarlez, J. Rheol. **50**, 975 (2006).
[51] D. Bouttes and D. Vandembroucq, AIP Conf. Proc. **1518**, 481 (2013).
[52] V. B. Nguyen, T. Darnige, A. Bruand, and E. Clement, Phys. Rev. Lett. **107**, 138303 (2011).
[53] E. N. da C. Andrade, Proc. R. Soc. London A **84**, 1 (1910).
[54] D. McLean, Rep. Prog. Phys. **29**, 1 (1966).
[55] J. Vermant, L. Walker, P. Moldenaers, and J. Mewis, J. Non-Newtonian Fluid Mech. **79**, 173 (1998).
[56] A. R. Jacob, A. S. Poulos, S. Kim, J. Vermant, and G. Petekidis, Phys. Rev. Lett. **115**, 218301 (2015).
[57] N. Koumakis and G. Petekidis, Soft Matter **7**, 2456 (2011).
[58] R. N. Zia, B. J. Landrum, and W. B. Russel, J. Rheol. **58**, 1121 (2014).
[59] G. Petekidis, J. Rheol. **58**, 1085 (2014).
[60] L. Ramos and L. Cipelletti, Phys. Rev. Lett. **94**, 158301 (2005).
[61] O. Lieleg, J. Kayser, G. Brambilla, L. Cipelletti, and A. R. Bausch, Nat. Mater. **10**, 236 (2011).
[62] A. Duri, P. Ballesta, L. Cipelletti, H. Bissig, and V. Trappe, Fluct. Noise Lett. **05**, L1 (2005).
[63] P. Hébraud and D. Lootens, Mod. Phys. Lett. B **19**, 613 (2005).
[64] D. Bi, J. Zhang, B. Chakraborty, and R. P. Behringer, Nature **480**, 355 (2011).
[65] M. D. Haw, Phys. Rev. Lett. **92**, 185506 (2004).
[66] M. E. Cates, J. P. Wittmer, J. P. Bouchaud, and P. Claudin, Phys. Rev. Lett. **81**, 1841 (1998).
[67] A. Tanguy, F. Leonforte, and J.-L. Barrat, Eur. Phys. J. E **20**, 355 (2006).
[68] A. Lemaître and C. Caroli, Phys. Rev. Lett. **103**, 065501 (2009).
[69] K. Martens, L. Bocquet, and J.-L. Barrat, Phys. Rev. Lett. **106**, 156001 (2011).
[70] E. E. Ferrero, K. Martens, and J.-L. Barrat, Phys. Rev. Lett. **113**, 248301 (2014).